PHYSOR 2004 -The Physics of Fuel Cycles and Advanced Nuclear Systems: Global Developments
Chicago, Illinois, April 25-29, 2004, on CD-ROM, American Nuclear Society, Lagrange Park, IL. (2004)

Ab Initio Generation of Thermal Neutron Scattering Cross Sections

A. I. Hawari, I. I. Al-Qasir, V. H. Gillette, B. W. Wehring, T. Zhou
Department of Nuclear Engineering, P.O. Box 7909, North Carolina State University, Raleigh, NC 27695-7909

Quantum mechanical ab initio (i.e., first principle) methods are applied in generating the thermal neutron scattering cross sections of moderators and reflectors that are of interest in nuclear technology. Specifically, this work focuses on graphite and beryllium. In both cases, the ab initio code VASP and the lattice dynamics code PHONON were used to generate the dispersion relations, and the phonon frequency distributions (density of states). This information was then utilized in the LEAPR module of the NJOY code to calculate the thermal neutron scattering cross sections at various temperatures. The use of the ab initio approach represents a major departure from previously applied methods, which depended mainly on fitting simpler dynamical models to experimental data to arrive at the phonon frequency distributions. In this case, much more complicated models of the atomic system of interest can be set up, which allows the establishment of a more complete dynamical matrix. As opposed to the semi-empirical methods used previously, this method represents a fundamental and predictive approach for estimating materials' properties including ones that are of interest in nuclear reactor design.

KEYWORDS: neutron, thermal neutron, slow neutron, ab initio, VASP, graphite, beryllium, moderator, phonon frequency distribution, thermal neutron scattering cross section, nuclear reactor

1. Introduction

Due to advances in computational power, the possibility now exists to perform detailed quantum mechanical ab initio (i.e., first principle) simulations of atomic systems. These simulations are currently used in fields such as physics, chemistry, and materials science to characterize and predict the behavior of new and exotic materials [1]. Using this approach, it is possible to establish the equilibrium atomic positions of a given material and predict the various properties of the material starting from such basic information as the coordinates of the atoms. Consequently, ab initio simulations seek to gain insight into the bonding forces in the material, which are usually variations of the Coulomb force that result in the formation of ionic, covalent, molecular, and van der Waals bonds.

In nuclear reactor design, the effect of atomic and/or molecular bonding becomes important as the neutrons slow down and enter the thermal (or slow) region (neutron energy $\leq$ 1 eV). The microscopic interaction (i.e., absorption, scattering, etc.) of slow neutrons within the reactor core defines the thermal neutron energy spectrum, which affects several global (macroscopic) properties such as criticality, and safety and feedback response. Therefore, the accuracy of the thermal neutron scattering cross sections that are used in reactor core design calculations are important for operating the reactor in an optimized and safe manner.

In the past, the thermal neutron scattering cross sections were derived from structure dynamics models that were fitted to experimental data in order to quantify the forces between the atoms and calculate the required excitation density of states [2]. However, by using the ab initio approach, the ability now exists to treat much larger systems of atoms, and arrive at more accurate and complete dynamical models from

which information relevant to the calculation of the thermal scattering cross sections can be derived. In addition, by utilizing the inherent predictive capability of this approach, investigation can be made of the use of new materials in the structure of the fuel [3] or the core in general. Furthermore, this also makes it possible to predict the changes in the neutronic properties of important core components due to exposure to radiation.

2. Low energy neutron scattering

Slow (Energy ≤ 1 eV) neutrons have de Broglie wavelengths that are comparable to the inter-atomic spacing of the scattering material. As a result coherent and incoherent scattering effects become possible. In addition, the kinetic energy of slow neutrons is comparable to the energy levels that can be excited in a scattering event (e.g., the vibrational levels in crystals). Therefore, thermal neutron cross sections will reflect the dynamics of the structure of the scattering material.

The typical start for the derivation of an expression that describes the scattering of a slow neutron from matter is to analyze the scattering event using time dependent perturbation theory, which implies the applicability of the Born approximation for describing the transition of a plane wave from a given initial state to a final state. Fermi's golden rule can then be applied to calculate the transition rate. However, for this analysis to be applicable, the neutron-nucleus interaction potential is assumed to be much shorter than the neutron wavelength, which allows it to be expressed by the well-known form of the Fermi pseudopotential. Based on these assumptions, the derivation of the expression for the double differential thermal neutron scattering cross section can be found in various standard references [4]. In compact form it can be represented by

$$\frac{d^2\sigma}{d\Omega dE} = \frac{1}{4\pi}\frac{k'}{k}\left(\sigma_{coh}S\left(\vec{Q},\omega\right)+\sigma_{inc}S_s\left(\vec{Q},\omega\right)\right), \tag{1}$$

where k and k′ represent the magnitude of the wave vector for the incoming and scattered neutron respectively, σ_{coh} is the bound atom coherent scattering cross section, and σ_{inc} is the bound atom incoherent scattering cross section. Notice that Eq. 1 can be taken to represent the microscopic or macroscopic cross section depending on the definition of σ_{coh} and σ_{inc}. Finally, $S(\vec{Q},\omega)$ is known as the scattering law, where $\vec{Q} = \vec{k} - \vec{k}'$ is the scattering vector and ω is the frequency. In general, S is composed of two terms as follows

$$S\left(\vec{Q},\omega\right) = S_s\left(\vec{Q},\omega\right)+S_d\left(\vec{Q},\omega\right), \tag{2}$$

where S_s is known as the self scattering law, which accounts for non-interference (incoherent) effects, while S_d is the distinct scattering law and accounts for interference (coherent) effects. Examination of Eq. 1 shows that the thermal neutron scattering cross section depends on two factors: first, the neutron-nucleus interaction as represented by the bound atom cross sections, and second, a factor that represents the dynamics of the scattering system (i.e., collection of atoms) as represented by the scattering law.

Using Van Hove's formulation, the scattering law is interpreted as the Fourier transform (in space and time) of the probability distribution functions that describe the correlated time dependent locations of the atoms. Therefore the scattering law can be written as

$$S\left(\vec{Q},\omega\right) = \frac{1}{2\pi\hbar}\int_{-\infty}^{\infty}\int G(\vec{r},t)e^{i(\vec{Q}.\vec{r}-\omega t)}d\vec{r}dt\,, \tag{3}$$

where $G(\vec{r},t)$ represents the probability of finding the atom at position $\vec{r}$ at time t and can be expressed in terms of self and distinct components as

$$G(\vec{r},t) = G_s(\vec{r},t) + G_d(\vec{r},t), \tag{4}$$

where G_s represents the probability of finding the same atom, and G_d represents the probability of finding a different atom $\vec{r}$.

Furthermore, if a harmonic approximation is introduced, where each atom in the scattering medium is assumed to be bound to other atoms by a harmonic force, an expansion can be performed that allows the decomposition of the scattering law into elastic and inelastic components. For crystals, this expansion is known as a phonon expansion. It can be performed on both the self and distinct components of the scattering law to get

$$\begin{aligned} S_s &= {}^0S_s + {}^1S_s + {}^2S_s + {}^3S_s + {}^4S_s + \ldots \\ S_d &= {}^0S_d + {}^1S_d + {}^2S_d + {}^3S_d + {}^4S_d + \ldots \end{aligned} \tag{5}$$

In this case, the terms that have the zero superscript represent 0 phonon creation (or annihilation), while the terms that have the higher superscripts represent the creation or annihilation of 1, 2, 3, etc. phonons. Therefore, the 0 term represents elastic scattering events, and the other terms represent inelastic scattering events. For example, the phenomenon of Bragg scattering, which represents coherent elastic scattering, is described by the ${}^0S_s$ term in Eq. 5. On the other hand, thermal neutron interactions in nuclear reactor cores include inelastic processes that are described by the higher order S_s and S_d terms.

The above formulation represents the basis of computer programs such as GASKET and LEAPR/NJOY [5-7], which are used to calculate thermal neutron scattering cross sections. These programs employ what is known as the incoherent approximation. In this case, the S_d component of the scattering law is set equal to zero. In addition, the S_s term is assumed to be based on a Gaussian-like G_s function. Using these approximations and defining the dimensionless momentum exchange variable α, and energy exchange variable β, the scattering law for cubic Bravais lattices can be written as

$$S(\alpha,\beta) = \frac{1}{2\pi}\int_{-\infty}^{\infty} e^{i\beta\hat{t}} e^{-\gamma(\hat{t})} d\hat{t}\,, \tag{6}$$

where $\gamma(\hat{t}) = \alpha\int_{-\infty}^{\infty} \frac{\rho(\beta)\left[1-e^{-i\beta\hat{t}}\right]e^{-\beta/2}}{2\beta\sinh\left(\beta/2\right)}d\beta$, $\alpha = \frac{E' + E - 2\mu\sqrt{E'E}}{Ak_BT}$, $\beta = \frac{E'-E}{k_BT}$, $\hat{t}$ is time in units of $\hbar/(k_BT)$ seconds, and $\rho(\beta)$ is the frequency spectrum of excitations of the scattering system (i.e., phonon density of states in a crystal), A is the atomic weight, k_B is Boltzman's constant, and T is the temperature of the scattering medium.

Based on the above, Eq. 1 is reduced to give the following form of the thermal neutron inelastic scattering cross section

$$\frac{d^2\sigma}{d\Omega dE} = \frac{\sigma_{coh} + \sigma_{inc}}{4k_BT}\sqrt{\frac{E'}{E}}S(\alpha,\beta), \tag{7}$$

where E, and E′ represent the initial and final energies, respectively, of the neutron.

3. Ab initio crystal dynamics

In general, the first step in establishing the phonon frequency spectrum for crystalline materials is to set up a dynamical matrix based on the crystal structure. For a 3-dimensional crystal that contains N unit cells and n atoms, the position of the i^{th} atom is defined as $\vec{R}_{L,i} = \vec{R}_L + \vec{r}_i$, Where $\vec{R}_L$ is the lattice vector, and $\vec{r}_i$ is the position vector of the i^{th} atom in the unit cell. The interaction with the j^{th} atom in unit cell L′ can be described by setting up the equation of motion that describes this interaction. Assuming harmonic behavior, an atom that is displaced by a small amount $\vec{u}_i(\vec{R}_L)$ form its equilibrium position, will experience a net force that can be described by

$$\vec{F}_i(\vec{R}_L) = -\sum_{\vec{R}_{L'},j} C_{\mu i,\nu j}(\vec{R}_L,\vec{R}_{L'})\cdot\vec{u}_j(\vec{R}_{L'}), \tag{8}$$

where the $C_{\mu i,\nu j}(\vec{R}_L,\vec{R}_{L'})$ terms represent the interatomic force constants and are given by

$$C_{\mu i,\nu j}(\vec{R}_L,\vec{R}_{L'}) = \left.\frac{\partial^2 E}{\partial u_{\mu i}(\vec{R}_L)\partial u_{\nu j}(\vec{R}_{L'})}\right|_0 . \tag{9}$$

μ and ν are indexes that take the values 1,2 and 3, which represent the Cartesian coordinates (x, y, and z) of the force components, respectively, and E is the potential energy of the crystal. The solution to Eq. 9 has the form of a traveling plane wave, which upon substitution in Eq. 8 results in the equations of motion given by

$$\omega^2(\vec{k})\vec{u}_i = \sum_j D_{ij}(\vec{k})\cdot\vec{u}_i . \tag{10}$$

$D_{ij}(\vec{k})$ is known as the dynamical matrix of the crystal, and has the form

$$D_{i,j}(\vec{k}) = \frac{1}{\sqrt{M_i M_j}}\sum_{\vec{R}_L} C_{\mu i,\nu j}(\vec{R}_L)\cdot e^{-i\vec{k}\cdot\vec{R}_L}, \tag{11}$$

where M is the mass of atom i or j. The relations $\omega(\vec{k})$ are known the dispersion relations, where for a crystal of n atoms per unit cell, there are 3n dispersion relations (also known as branches). Three of the branches represent acoustical modes; while 3n-3 represent optical modes. By randomly sampling $\vec{k}$ over the Brillouin zone, the phonon frequency distribution spectrum (density of states) can be constructed [8].

Solution of the above equations requires knowledge of the interatomic force constants, which in turn requires the calculation of the total potential energy of the crystal. Traditionally, these force constants were determined by fitting the dispersion relations and/or other themodynamical function to experimental data [2]. This approach suffers from two major deficiencies. The first is that it is not predictive, producing atomic force constants and dispersion relations that are inferred from experimental data. The second is that the results are not unique and can possibly be reproduced by alternative dynamical models.

However, in the ab initio approach, the ground state energy of the crystal is calculated explicitly and used in Eq. 8 to evaluate the force constants. In this case, the Born-Oppenheimer approximation allows the movement of electrons and ions to be decoupled. Consequently, Khon-Sham theory [9] can be used to develop a set of Schrödinger-like equations given by

$$\left(\frac{-\hbar^2}{2m_e}\nabla^2 + V_{ion-ele.} + V_H + V_{XC}\right)\psi_m = \varepsilon_m \psi_m, \tag{12}$$

Where ψ_m is the electronic wave function, ε_m is the Kohn-Sham eigenvalue, V_H is the Hartree potential of the electrons, and V_{XC} is the exchange-correlation potential, which is determined using the so-called Local Density Approximation (LDA) [1,9,10]. $V_{ion-ele.}$ is described using pseudopotential theory [11], which replaces the strong electron-ion potential with a much weaker pseudoptentil that describes all the features of the valence electrons moving through the solid, including relativistic effects. Thus, the original solid is now replaced by pseudo valence electrons and pseudo-ion cores. To relate the total energy calculated by the Kohn-Sham equation to the force constants, the Hellman-Feynman theorem is applied [12], which states that for any perturbation λ

$$\frac{\partial\langle E\rangle}{\partial\lambda} = \left\langle\psi\left|\frac{\partial H}{\partial\lambda}\right|\psi\right\rangle, \tag{13}$$

where H is the Hamiltonian of the system. If λ represents an atomic displacement, $u_{\alpha i}(\vec{R}_L)$, then the second derivatives of the energy are related to the matrix of the force constants by

$$\frac{\partial\langle E\rangle}{\partial u_i(\vec{R}_L)} = -\sum_{\vec{R}_{L'},j} C_{\mu i,\nu j}(\vec{R}_L,\vec{R}_{L'})\cdot\vec{u}_j(\vec{R}_{L'}), \tag{14}$$

which is simply a restatement of Eq. 1.

4. Calculation of thermal neutron scattering cross sections

The approach described above was implemented to calculate the thermal neutron scattering cross sections for beryllium and graphite. Figure 1 below shows the unit cell for both materials. Both beryllium and graphite belong to the space group P6_3/mmc. Beryllium has a hexagonal closed packed structure with two atoms per unit cell located at (1/3,2/3,1/4), and (2/3,1/3,3/4) the lattice constants values are a = b = 2.29 Å, and c = 3.58 Å. Graphite has a hexagonal unit cell with four atoms per unit cell located at (0,0,0), (1/3,2/3,1/4), (0,0,3/4) and (2/3,1/3,3/4), the lattice constants have values a = b = 2.45 Å, and c= 6.68 Å. Unlike Be, graphite has a unique structure due to its very long c-axis. Strong covalent bonding exits between graphite interplaner atoms, while the intraplaner bonding (i.e., between the carbon sheets) is of the weak van der Waals type. The planes are stacked in an "abab" sequence. Consequently, this will yield both very low and very high frequency contributions to the density of states.

The calculations of the dispersion relations were performed using the Vienna Ab Inition Simulation Package (VASP) and the PHONON code [13,14]. The beryllium calculations utilized the generalized gradient approximation (GGA), which accounts for variations in the electron density. The projector augmented wave (PAW) pseudopotential was implemented assuming a 4x4x3 supercell (96 atoms). the

integration over the Brillouin zone was confined to a 4x4x4 k-mesh points generated by the Monkhrust-Pack scheme. The Hellmann-Feynman forces were computed from 3 independent displacements along x, y and z, each displacement generating 288 force components, for a total of 864 components. Figure 2 shows the ab initio based dispersion relations for beryllium metal (Be) compared to data generated using neutron scattering experiments [15]. Six vibrational modes appear in the figure as expected for the beryllium unit cell, which has 2 atoms. The lowest three branches, starting from Γ, are known as the acoustic modes, while the highest three branches are the optical modes. To compare to measurement, the dispersion relations are calculated along the high symmetry directions (Γ, K, M, H, and L) in the hexagonal Brillouin zone. As it can be seen, the agreement between measurement and calculation is excellent. This clearly illustrates the capabilities of the ab initio technique and the accuracy of the models used in this calculation.

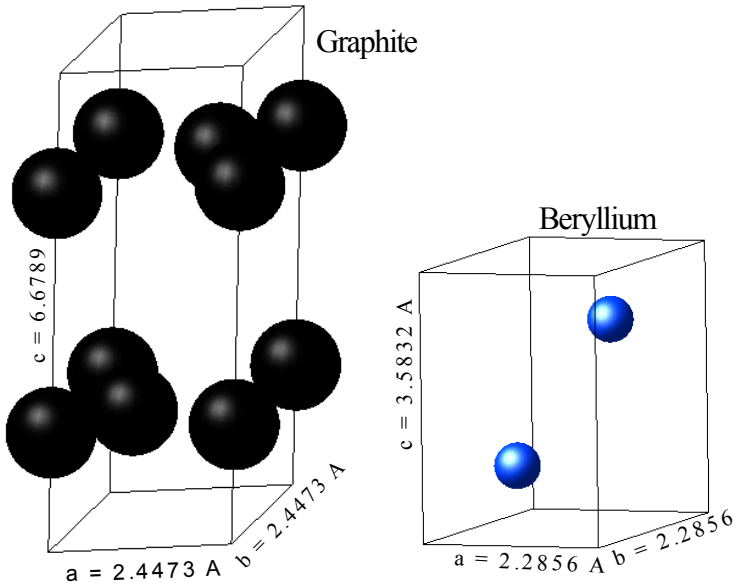

Fig. 1. Beryllium and graphite unit cells. Graphite has 4 atoms per unit cell, while beryllium has 2 atoms. The c-axis dimension for graphite is nearly twice that for beryllium.

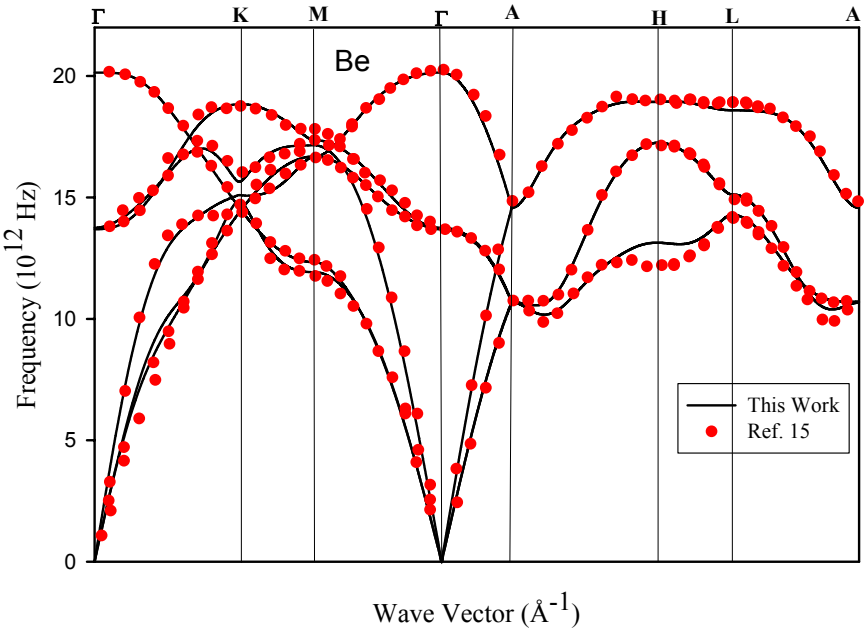

Fi.g. 2. The dispersion relations for beryllium based on a 96-atom supercell.

Once the dispersion relations ($\omega(\vec{k})$) are known, the phonon frequency distribution was constructed by randomly sampling $\vec{k}$ over the Brillouin zone. Figure 3 shows a comparison of the phonon frequency distribution for beryllium generated using ab initio methods and the one used in current calculations of the thermal scattering cross sections [5]. The agreement is reasonable, especially in the low energy region that is of interest in the thermal scattering calculations.

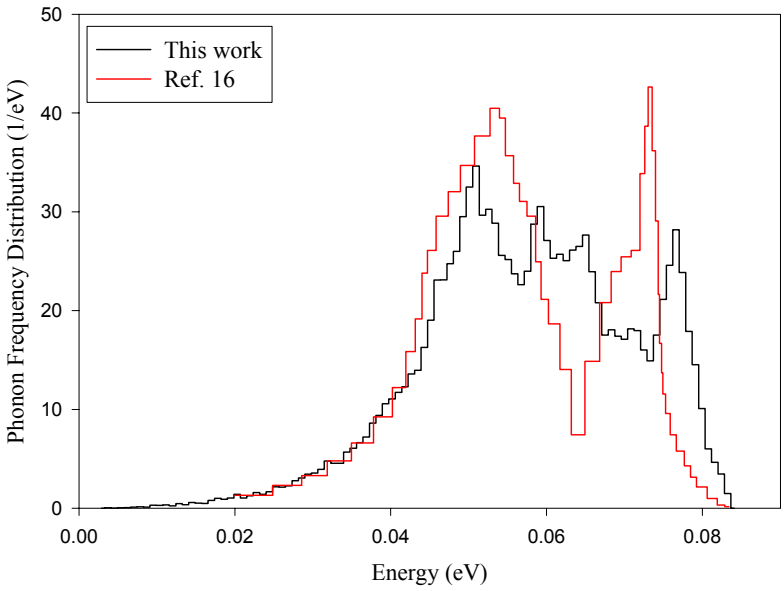

Fig. 3. The phonon frequency distribution for beryllium.

Based on the data in Fig. 3, the LEAPR module of the NJOY code was used to generate the beryllium thermal neutron scattering cross sections at a temperature of 300 K [5]. It can be seen that at energies below 0.1 eV the values of the cross section are slightly lower than ones that are commonly used [5], but for energies below the Bragg cut-off (~ 0.002 eV), they are closer to experimental data.

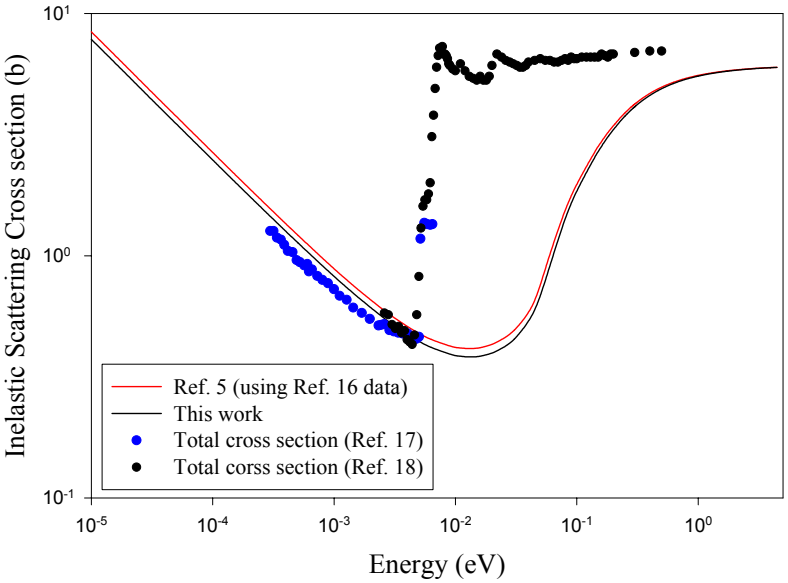

Fig. 4. The thermal neutron scattering cross sections for beryllium at 300 K.

The ab initio calculations of graphite were carried out using the local density approximation (LDA), and with the projector augmented wave (PAW) pseudopotential implemented by VASP. The VASP/PHONON model used a 6x6x1 supercell composed of 144 atoms. The integration over the Brillouin zone was confined to a 3x3x4 k-mesh generated by the Monkhrust-Pack scheme. The Hellmann-Feynman forces were computed from 6 independent displacements along x, y and z, each displacement generating 432 force components, for a total of 2592 components. Figure 5 shows the dispersion relations along the highest symmetry points of the Brillioun zone (A, Γ, M, K, and Γ). Twelve vibrational modes appear in the figure as expected for the graphite unit cell, which has 4 atoms. The lowest three branches, starting from Γ are the acoustical modes, while the highest three branches are the optical modes. For comparison, the figure also shows experimental data that were obtained through various techniques. As it can be seen, the agreement is remarkable and clearly illustrates the power and utility of the ab initio approach.

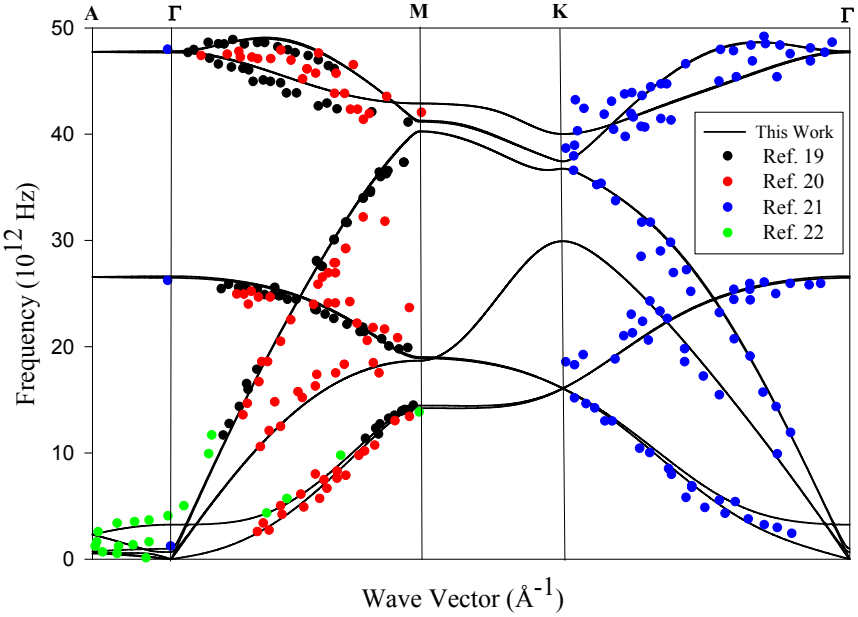

Fi.g. 5. The dispersion relations for graphite based on a 144-atom supercell.

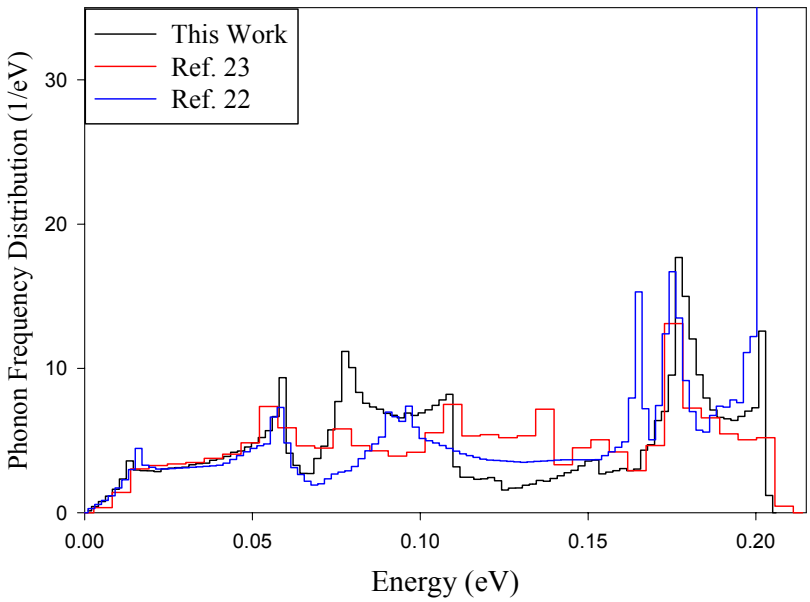

Fig. 6. The phonon frequency distribution for graphite.

Figure 6 shows the phonon frequency distribution for graphite. Clearly, graphite has a much wider distribution than beryllium. The figure also shows a comparison of the ab initio phonon frequency distribution of graphite to ones used in current calculations of the thermal scattering cross sections. The agreement is reasonable, especially in the low energy region that is of interest in the thermal scattering calculations. Finally, Fig. 7 below shows the calculated thermal neutron scattering cross sections for graphite using ab initio methods at temperatures of 300 and 1200 K. The comparison to the data used in Ref. 5 reveals differences that can reach approximately 100 % at energies around 0.02 eV. This is consistent with the higher phonon frequency values for the ab initio distribution in that energy region (see Fig. 6). Currently, published experimental data is being evaluated to compare to the calculated results. In addition, an integral benchmark experiment that uses the pulsed slowing-down-time technique has been planned to validate the graphite cross sections [24].

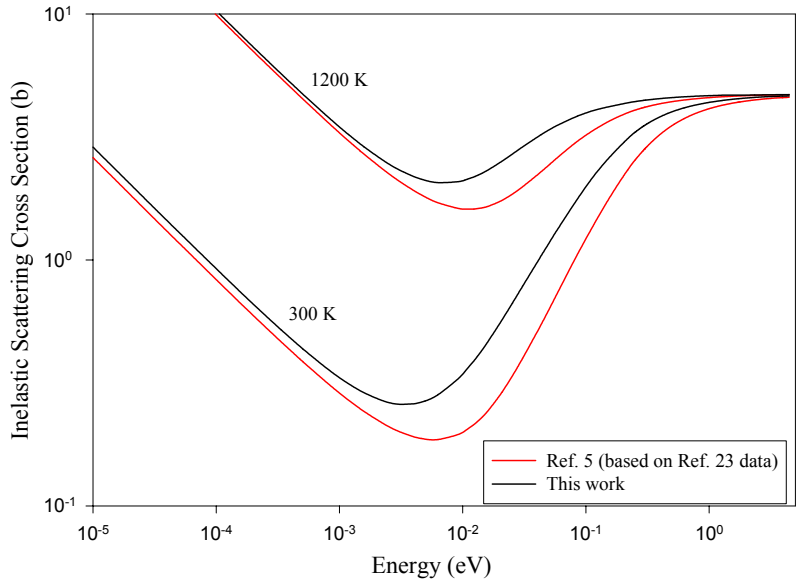

Fig. 7. The thermal neutron scattering cross sections for graphite at 300 and 1200 K.

5. Conclusions

Ab initio methods were used to calculate the fundamental dispersion relations, and generate the phonon frequency distributions for graphite and beryllium. Specifically, the VASP and PHONON codes were implemented. In both cases, the dispersion relations show excellent agreement with experimental data. Using the ab initio phonon frequency distributions, the LEAPR/NJOY code system was used to generate the thermal neutron scattering cross section of graphite and beryllium. In the case of beryllium, the ab initio calculated cross sections were comparable (slightly less) than the ones currently used in standard libraries, which is expected based on the similarities of the phonon frequency distributions at low energy. However, in the case of graphite the differences can reach 100% at energies characteristic of slow neutrons, which is consistent with the observed differences in the ab initio and Young –Koppel (Ref. 23) phonon frequency distributions at low energy. In this case, comparison to published experimental data is underway. In addition, an integral benchmark experiment that uses the pulsed slowing-down-time technique has been planned to validate the graphite cross sections

Acknowledgments

This work was supported by the U.S. Department of Energy under grant No. DE-FG03-02SF22514.

References

1) K. Ohno, K. Esfarjani, and Y. Kawazoe, "Computational Material Science from Ab Initio to Monte Carlo Methods," Springr-Verlag, Berlin, Heidelberg (1999).
2) T. Paszkiewics, " Physics of Phonons," Springer-Verlag, Berlin, Heidelberg (1987).
3) I. I. AL-Qasir, A. I. Hawari, V. H. Gillette, B. W. Wehring, and T. Zhou, "Thermal Neutron Scattering Cross Sections of Thorium Hydride," PHYSOR 2004, Chicago, IL, USA, 2004.
4) G. L. Squires, "Introduction to the Theory of Thermal Neutron Scattering," Cambridge University Press, Cambridge, UK (1977).
5) R. E. MacFarlane, "New Thermal Neutron Scattering Files for ENDF/B-VI, Release 2," LA-12639-MS, Los Alamos National Laboratory (1994).
6) R. E. MacFarlane, and D. W. Muir, "The NJOY Nuclear Data Processing System, Version 91," LA-12740-MS, Los Alamos National Laboratory (1994).
7) J. U. Koppel, J. R. Triplett, and Y. D. Naliboff, "GASKET: A Unified Code for Thermal Neutron Scattering," General atomic report GA-7417(Rev.) (1967).
8) M. T. Dove, "Introduction to Lattice Dynamics," Cambridge University Press, Cambridge, UK (1993).
9) W. Kohn and L. J. Sham, Phys. Rev., **140**, A1133 (1965).
10) J. P. Perdew, and A. Zunger, Phys. Rev. B, **23**, 5084 (1981).
11) J. C. Phillips, and L. Kleinman, Phys. Rev., **116**, 287, (1959).
12) R. P. Feynman, Phys. Rev., **56**, 340, (1939).
13) G. Kresse, and J. Furthmuller, "Vienna Ab-Initio Simulation Package, VASP the Guide," Vienna, 2002.
14) K. Parlinski, "PHONON manual, version 3.11," Krakow, 2002.
15) M. Lazzeri, and S. De Gironcoli, Surf. Sci., 402-404, **715**, (1998).
16) J. A. Young, and J. U. Koppel, Phys. Rev., **6**, A1476, (1964).
17) D. J. Hughes, and R. B. Schwartz, "Neutron Cross Sections-BNL325", second edition, 95, (1958).
18) K. Kanda, and O. Aizawa, J. of Nuclear Science and Technology, 12 (10), 601, (1975).
19) J. L. Wilkes, R. E. Palmer and R. F. Willis, J. Electron Spectrosc. Relat. Phenom. **44**, 355, (1987).
20) C. Oshima, T. Aizawa, R. Souda, Y. Ishizawa and Y. Sumiyoshi, Solid State Commun. **65**, 1601 (1988).
21) G. Benedek, F. Hofman, P. Ruggerone, G. Onida and L. Miglio, Surf. Sci. Rep., **20**, 1 (1994)
22) R. M. Nicklow, N. Wakabayashi and H. G. Smith, Phys. Rev. B, **5**, 4951 (1972).
23) J. A. Young, and J. U. Koppel, J. Chem. Phys., **42**, 357 (1965).
24) T. Zhou, A. I. Hawari, B. W. Wehring, I. I. Alqasir, V. H. Gillette, F. C. Difilippo, J. P. Renier, "Utilizing The Oak Ridge Electron Linear Accelerator Facility For Benchmarking Neutron Thermalization in Moderators," AccApp'03, San Diego, CA, USA, 2003.